Carbon monoxide binding properties of domain-swapped dimeric myoglobin

Satoshi Nagao • Haruto Ishikawa • Takuya Yamada • Yasuhisa Mizutani • Shun Hirota

S. Nagao • T. Yamada • S. Hirota (✉)

Graduate School of Materials Science, Nara Institute of Science and Technology, 8916-5, Takayama, Ikoma, Nara 630-0192, Japan

E-mail: hirota@ms.naist.jp; Fax: +81-743-72-6119, Tel: +81-743-72-6110

H. Ishikawa · Y. Mizutani

Department of Chemistry, Graduate School of Science, Osaka University, 1-1 Machikaneyama, Toyonaka 560-0043, Japan

Abstract

Myoglobin (Mb) is a monomeric oxygen storage hemoprotein, and has been shown to form a domain-swapped dimer. Monomeric and dimeric carbon monoxide (CO)-bound Mb (MbCO) exhibited similar absorption spectra. In this study, the CO stretching frequencies of MbCO were observed at 1932 and 1944 cm^{-1} for both monomeric and dimeric MbCO. The resonance Raman (RR) bands for the stretching between the heme iron and axial ligands were observed at the same frequencies for the monomer and dimer of deoxygenated Mb (deoxyMb) and MbCO, respectively ($\nu_{Fe–His}$, 220 cm^{-1}; $\nu_{Fe–C}$, 507 cm^{-1}), showing that the Fe–His bond strength of deoxyMb and the Fe–CO bond strength of MbCO did not change by the dimerization. Time-resolved RR measurements showed that the dynamics of the structural changes at the heme active site after CO photo-dissociation of MbCO was similar between monomeric and dimeric Mb (monomer, (5.2 ± 1.8) x 10^6 s^{-1}; dimer, (6.2 ± 1.1) x 10^6 s^{-1} at room temperature). These results show that the heme coordination structure, the protein environment around the bound CO, and the protein relaxation character are similar between monomeric and dimeric MbCO. Although the active site structure was similar between the monomer and dimer, the CO binding rate constant of dimeric Mb ((1.01 ± 0.03) x 10^6 $M^{-1}s^{-1}$ at 20°C) was about twice larger than that of the monomer ((0.52 ± 0.02) x 10^6 $M^{-1}s^{-1}$ at

20°C), presumably due to the expansion of the channel between the Xe3 cavity and the solvent by the dimerization.

Keywords

Myoglobin • Domain swapping • Ligand binding • Active site structure

Introduction

Elucidation of the structure–function relationship of proteins is indispensable for understanding the molecular mechanism of proteins. Myoglobin (Mb) is a monomeric oxygen storage hemoprotein, which has been used as a model protein to study the structure–function relationship of proteins [1-5]. Mb consists of 153 amino acids with eight α-helices (A to H helices) and seven non-helical segments (**Fig. 1A**) [6, 7]. His93 of the F-helix coordinates to the heme iron (**Fig. 1B**), whereas His64 of the E-helix creates a hydrogen bond with the bound oxygen and stabilizes the oxygenated form. Recently, we have shown that dimeric horse metMb forms a unique domain-swapped structure (**Fig. 1C**) [8]. Domain swapping has also been detected in other hemoproteins [9-14]. Domain swapping is an oligomerization mechanism for proteins, where a protein molecule exchanges its domain or secondary structural element with another molecule [15-17]. In dimeric metMb, a new long α-helix is formed by the E and F helices and the EF-loop of the original monomer, and as a result His93 and His64 in the heme active site originate from different protomers (**Fig. 1D**) [8]. The relative positions of the amino acid residues were similar between the monomer and dimer except for the EF-loop. Interestingly, the O_2 binding rate constant (k_{on}) of the dimer was similar to that of the monomer, although the O_2 dissociation rate constant

(k_{off}) was slightly smaller [8].

Carbon monoxide (CO)-bound Mb (MbCO) has been frequently used as a model system for elucidating the ligand binding properties in detail, since MbCO is more stable than oxygenated Mb (MbO_2) [3, 18-35]. The CO stretching (ν_{CO}) frequency of MbCO can be observed by infrared (IR) spectroscopy, and its frequency is a sensitive probe of the distal pocket environment [36, 37]. The major factor governing the ν_{CO} frequency is not the steric hindrance but the electrostatic potential surrounding the CO [20]. Resonance Raman (RR) spectroscopy is a useful tool for elucidating the tertiary and quaternary structures of hemoproteins by monitoring the vibrational modes of the heme [2, 38-46].

It has been reported that CO binds to sperm whale Mb much slower than O_2 [22]. The difference in the ligand binding kinetics of CO and O_2 have been attributed to the differences in the energy barriers for CO and O_2 on geminate rebinding and ligand escape to the solvent [47, 48]. Since the inner kinetic barrier for heme iron–CO bond formation is about twice as large as that of CO escaping to the solvent, the rate-limiting step for CO binding is the bond formation between the heme iron and CO [22, 48]. The quantum efficiency of CO photo-dissociation is very high for Mb [49]. Therefore, CO photo-dissociation of Mb has been used to investigate its ligand migration pathway

[27-32, 35] and protein structural changes during ligand binding [43, 50-53]. It has been shown by time-resolved Laue crystallography that CO molecules are localized in Mb at its internal cavities (Xe1–Xe4) at nanosecond to millisecond time scale after CO photo-dissociation [27-29]. The pathway from the distal pocket to the Xe3 cavity including the Xe1, Xe2, and Xe4 cavities of Mb has been proposed as the major CO migration pathway at cryogenic temperatures [30, 31]. An alternative ligand binding pathway has been suggested for Mb by structure characterization with binding of large ligands [54-57] and mutagenesis mapping experiments [58-60], where the distal His64 creates a channel. Molecular dynamics study has also uncovered another possible ligand pathway with hydrophobic channels between the E and B or H and G helices [61]. To gain more information on the relationship between the active site structure and ligand binding properties in Mb, the CO binding properties were compared between monomeric and dimeric MbCO. The active site structure, as well as the protein dynamics after CO photo-dissociation, was similar between monomeric and dimeric MbCO. However, the k_{on} value of CO binding for dimeric Mb was higher than that for the monomer. These results indicate that the CO migration property is different between the monomer and dimer, although the active site structure is similar between them.

Materials and methods

Preparation of Monomeric and Dimeric Mb. Dimeric horse metMb was prepared by the method reported previously [8]. After the dimeric metMb solution was filtrated, dimeric metMb was purified by gel chromatography (HiLoad 26/60 Superdex75, GE healthcare) using a fast protein liquid chromatography (FPLC) system (BioLogic DuoFlow 10, Bio-Rad, CA) with 50 mM potassium phosphate buffer, pH 7.0. The concentration of dimeric metMb was calculated from the absorbance at 408 nm with an extinction coefficient of 188 $mM^{-1}cm^{-1}$ [8], and adjusted to desired concentrations. The solution of purified dimeric metMb was degassed with a vacuum line and subsequently flushed with N_2, followed by an anaerobic addition of dithionite (10 equivalents to metMb) under CO atmosphere. Monomeric horse metMb was prepared by dissolving horse heart metMb (Sigma) in the same buffer. Monomeric MbCO was prepared by the same procedure as dimeric MbCO.

Optical Absorption and CD Measurements. Absorption spectra were measured with a UV-2450 spectrophotometer (Shimadzu, Japan) at 20 °C using a 1-cm path-length quartz cell. Circular dichroism (CD) spectra were measured with a J-725 CD spectropolarimeter (Jasco, Japan) at 20 °C using a 0.1-cm path-length quartz cell.

FT-IR Measurements. IR spectra of monomeric and dimeric horse MbCO were

measured at room temperature with a FT-IR spectrometer (FT/IR-6100 TRV, JASCO, Japan) equipped with an MCT detector (SDU-6000MCT, JASCO, Japan). MbCO (500 μM, heme unit) in 50 mM potassium phosphate buffer, pH 7.0, was loaded to a gas-tight IR-transmittance 20 μm cell with CaF_2 windows and a Teflon spacer. After loading the sample to the cell, the cell was placed in the FT-IR spectrometer, which was purged continuously with N_2. Spectral data were collected at 2-cm^{-1} resolution and averaged with 512 scans. The spectrum of MbO_2 was measured, and subtracted from that of MbCO. Gaussian fitting was performed using the Igor Pro ver. 6.0 program (WaveMetrics, Portland) for the ν_{CO} band of MbCO, where the peak positions of the ν_{CO} bands were fixed to the reported frequencies [20].

Resonance Raman Measurements. Nanosecond time-resolved resonance Raman (RR) measurements of monomeric and dimeric horse MbCO were performed at room temperature with two nanosecond-pulse lasers operating at 1 kHz. The probe pulse at 436 nm was obtained as the second harmonic of the output of an Nd:YLF-pumped Ti:sapphire laser (Photonics Industries, TU-L). The power of the probe pulse was set as low as possible (1.0 μJ/pulse) in order to avoid ligand photolysis. The pump pulse at 532 nm was generated with a diode-pumped Nd:YAG laser (Megaopto, LR-SHG), and the power was adjusted to 185 μJ/pulse. The pulse widths of

the pump and probe pulses were 20 and 25 ns, respectively. The delay time of the pump and probe pulse was -50 - 500 ns. The pump and probe beams were aligned collinearly using a dichroic mirror, and focused to the sample cell with spherical and cylindrical lenses. The timing between the pump and probe pulses was adjusted with a computer-controlled pulse generator (Stanford Research Systems, DG 535) with a GPIB interface. The time delay of the probe pulse with respect to the pump pulse was determined by detecting the two pulses with a photodiode (Electro-Optics Technology, ET-2000) placed before the sample point and monitored with an oscilloscope (Iwatsu, Waverunner DS-4262). The jitter in the delay time was within ±5 ns.

Monomeric and dimeric horse MbCO (75 μM, heme unit) solutions were transferred into an airtight 10-mm diameter NMR tube, which was spun with a spinning device designed to minimize the off-center deviation during rotation. The Raman scattered light was detected with a liquid N_2-cooled charge-coupled device camera (Roper Scientific, Spec-10:400B/LN) attached to a custom-made prism prefilter (Bunko Keiki) equipped with a single spectrograph (HORIBA, iHR550). The spectra were calibrated using the spectra of cyclohexane and carbon tetrachloride. Gaussian fitting was performed using the Igor Pro ver. 6.0 program (WaveMetrics, Portland) for the γ_7 band after CO photo-dissociation of MbCO, where the peak positions of the γ_7 bands

were fixed to 294.2 and 306.6 cm^{-1} for the monomer, and 292.7 and 306.6 cm^{-1} for the dimer.

Monomeric and dimeric horse deoxyMb solutions were prepared by reduction of the corresponding metMb with dithionite (10 equivalents to metMb) under N_2 atmosphere. Monomeric and dimeric deoxyMb (monomer, 75 μM; dimer, 100 μM, heme unit) solutions were transferred into an airtight 10-mm diameter NMR tube, and the RR spectra were measured with the probe beam only.

Laser Flash Photolysis Measurements. The concentration of monomeric and dimeric horse MbCO was adjusted to 8 μM (heme unit). The sample solution was transferred to a sealed quartz cell, which was filled with a mixture of CO and N_2 using a gas mixer (MX-3S, Crown, Tokyo). The partial pressure of CO was varied from 20 to 100%. Each measurement was performed after incubation for at least 30 min at 20 °C to equilibrate Mb with CO. To obtain the rate constant of CO binding to deoxyMb, flash photolysis of MbCO was performed using the second harmonic (532 nm) of a Nd:YAG laser (Surelight I-10, Continuum, Santa Clara; pulse energy, 5 mJ; pulse width, 5 ns; pulse frequency, 10 Hz) for excitation. Time-resolved absorbance changes at 435 nm were measured at 20 °C with illumination from a Xe lamp orthogonal to the laser pulse and recorded on a digital oscilloscope (TDS 3012B, Tektronix, Tokyo), which received

voltage signals from the photomultiplier attached to a monochromator (RSP-601-03, Unisoku, Osaka). The traces were obtained as averages of 32 pulses.

Results

No dissociation of domain-swapped dimeric horse Mb to monomers was observed in the size exclusion chromatogram for the solution after reduction of dimeric metMb with dithionite and subsequent binding of CO to Mb (**Fig. S1**). These results show that dimeric metMb did not dissociate to monomers during preparation of MbCO, which allowed a further investigation of dimeric MbCO. The maximum wavelength of the MbCO Soret band at 423 nm did not change by the dimerization (**Fig. 2A**). The wavelengths of the maximum absorbance of the Q-bands in the optical absorption spectra were the same between the monomer and dimer (**Fig. 2A**). However, the intensities of the 208 and 222-nm α-helix-related negative bands in the CD spectra increased by the dimerization of MbCO, in which the increase in the α-helical content was estimated to be about 12% (**Fig. 2B**). These results indicate that the active site structure was similar between monomeric and dimeric MbCO, although the secondary structure was slightly different between them.

We measured the FT-IR and RR spectra of the monomer and dimer of MbCO

and deoxyMb to investigate the environment of the distal pocket around the bound CO (**Figs. 3 and S2**) [20, 62]. The spectra obtained by addition of the deconvoluted Gaussian bands of the ν_{CO} band fitted well to the spectra observed experimentally (**Fig. 3**). The peak wavelengths of the deconvoluted ν_{CO} bands were 1932 and 1944 cm^{-1} for both the monomer and dimer, whereas the area ratios of the bands at 1932 and 1944 cm^{-1} were estimated as 3:7 and 2:8 for the monomer and dimer, respectively. These results support the hypothesis that the environment of the distal pocket around the bound CO was similar between the monomer and dimer. The band observed at 220 cm^{-1} in the RR spectra of monomeric deoxyMb has been assigned to the heme iron−His93N_{ε} stretching mode ($\nu_{Fe–His}$) (**Fig. 4A**) [63, 64]. The $\nu_{Fe\text{-}His}$ frequency of dimeric deoxyMb was also observed at 220 cm^{-1}. The band observed at 507 cm^{-1} in the RR spectrum of monomeric MbCO has been assigned to the Fe–CO stretching mode ($\nu_{Fe–C}$) (**Fig. 4B**) [40]. The frequency of the $\nu_{Fe–C}$ band also did not change by the dimerization of MbCO (**Fig. 4B**). These results show that the Fe–His bond strength of dimeric deoxyMb and the Fe–CO bond strength of dimeric MbCO are similar to the corresponding bond strengths of the monomer.

Nanosecond time-resolved RR spectra after CO photo-dissociation for monomeric and dimeric MbCO were compared to investigate the difference in protein

structural changes in the monomer and dimer (**Figs. 5A and 5B**). RR bands were observed at 220, 304, and 342 cm^{-1} in the spectra of the CO-dissociated monomeric and dimeric Mb. The bands at 304 and 342 cm^{-1} have been assigned to the methine wagging out-of-plane (γ_7) and iron−pyrrole stretching in-plane skeletal (ν_8) modes, respectively [40]. These characteristic bands of deoxyMb have been used to evaluate the structural changes of the active site [40, 50, 51, 53]. The peak area of the γ_7 band changed gradually in sub-microsecond order after CO photo-dissociation (**Figs. 5C and 5D**). The relaxation rate constant was obtained by exponential fitting of the γ_7 peak area (**Figs. 5C and 5D inset**), where the rate constants were obtained as (5.2 ± 1.8) x 10^6 and (6.2 ± 1.1) x 10^6 s^{-1} for the monomer and dimer, respectively. Since the rate constants were similar between the monomer and dimer, the dynamics of the structural changes at the heme active site after CO dissociation were similar between the monomer and dimer, which was consistent with the results of the ν_{CO} and ν_{Fe-C} frequencies (**Fig. 4**).

CO rebinding kinetics were measured as a function of CO concentration to investigate the CO binding properties of monomeric and dimeric Mb. About a half of MbCO reacted and the deoxy protein was produced by the photolysis according to the initial absorbance change. The observed rate constants (k_{obs}) increased linearly as a function of CO concentration, as expected for a simple rebinding phenomenon [19].

From the plots of k_{obs} versus [CO] (**Fig. 6**), k_{on} is calculated using eq. 1.

$$k_{obs} = k_{on}([\text{deoxy heme}]+[\text{CO}]) + k_{off} \quad (1)$$

[deoxy heme] and [CO] represent the concentrations of deoxy heme and CO at the final equilibrium, respectively. Under our experimental conditions, CO is in large excess with respect to Mb ([CO] ≥ 210 μM, $[\text{Mb}]_{total}$ (heme unit) = 8 μM at 20°C), hence the term [deoxy heme] can be neglected in eq. 1, and the observed rebinding rate depends linearly on the CO concentration. The k_{on} value of the dimer was obtained as (1.01 ± 0.03) x 10^6 $M^{-1}s^{-1}$, which was about twice as large as that obtained for the monomer ((0.52 ± 0.02) x 10^6 $M^{-1}s^{-1}$).

Discussion

The absorption spectrum of Mb exhibits characteristic Soret and Q-bands depending on its coordination structure [1]. The Soret and Q-bands of dimeric MbCO corresponded well to those of monomeric MbCO (**Fig. 2A**). The ν_{CO} bands were observed at 1932 and 1944 cm^{-1} and their intensity ratio was 3:7 for monomeric MbCO (**Fig. 3A**), where similar frequencies and ratio have been reported for CO-bound sperm

whale Mb [20]. The ν_{CO} bands were also observed at 1932 and 1944 cm^{-1} and the intensity ratio of these bands was similar (2:8) for dimeric horse MbCO (**Fig. 3B**). The frequency of the ν_{CO} band reflects sensitively the environment around the bound CO in MbCO [20, 37]. Therefore, these results show that the heme coordination structure and the environment around the bound CO do not change by the dimerization of Mb. No significant difference in the frequencies of the ν_{Fe-His} band in the deoxy form and the ν_{Fe-C} band in the CO-bound form of Mb were observed between the monomer and dimer (**Fig. 4**), indicating that the Fe–His and Fe–CO bond structures did not change by the dimerization. The observed change showed that Mb adopts a metastable structure within a few picoseconds after CO dissociation, and the metastable structure may undergo structural changes in the submicrosecond time scale. The present study reveals the temporal change of the γ_7 band, which was not indicated in the previous study [43]. The metastable structure is characterized by exhibiting a higher γ_7 frequency compared to the deoxy form. The present time-resolved RR results indicate that monomeric and dimeric Mb form a similar metastable structure after CO photo-dissociation, and undergo similar structural changes with a similar kinetic constant (**Fig. 5**). The RR results in addition to the absorption and FT-IR results show that the active site structure was similar between monomeric and dimeric Mb in solution. It is noteworthy that the

active site structure and the protein structural dynamics after CO photo-dissociation were similar between monomeric and dimeric Mb, even though the E and F helices were exchanged between the protomers in the dimer.

The CO binding rate constant of the dimer was twice larger than that of the monomer, suggesting that the binding pathway is different between monomeric and dimeric Mb, although it has been reported that the k_{on} value for O_2 binding is similar between them [8]. The positions of the amino acid residues of the distal pocket (Leu29, Phe43, His64, and Val68) were similar between monomeric and dimeric Mb (**Fig. 7**). The positions of the side chains of Leu69, Leu72, Leu76, Leu89, His93, Leu104, Ile111, Leu135, and Phe138 located around the Xe1, Xe2, and Xe4 cavities were also similar between the monomer and dimer. However, the positions of Trp7, His82, and Leu137 located between the Xe3 cavity and the solvent were shifted by the dimerization of Mb (**Fig. 7**). As a result, the channel of the ligand migration between the Xe3 cavity and the solvent is broadened in the dimer compared to the monomer. An increase in the size of a channel may make the ligand migrate faster among the cavities and solvent, and thus we attribute the increase in the k_{on} value of CO binding by the dimerization to the expansion of the channel between the Xe3 cavity and the solvent. On the other hand, the k_{on} value for O_2 binding of the dimer has been shown to be similar to that of the

monomer [8], despite of expansion of the channel. These results suggest that the properties of the ligand migration is different between CO and O_2. The ligand pathway through the Xe1-Xe4 cavities may be more prominent in the migration of CO compared to that of O_2, and the His64 gate may be the major migration pathway for O_2 [60].

Comparison of the ligand binding properties between domain-swapped dimeric Mb and intrinsically tetrameric hemoglobin (Hb) may provide information on designing oligomeric proteins. The structure and ligand binding properties of both heme active sites of dimeric Mb were similar to those of monomeric Mb (**Figs. 2-4, 6, and S2**). Although the structure and ligand binding properties of the four heme active sites are similar in Hb, those of each heme site are affected by the structural change at other heme sites upon binding of a ligand, making Hb exhibit coorperativity [65]. The information of the structural change at the proximal site of a heme is transferred to the proximal site of other hemes in Hb [65]. However, dimeric Mb did not exhibit coorperativity, although the proximal site (His93) of each heme was connected directly with a long α-helix to the distal site (His64) of the other heme [8]. It may be difficult to transfer the information of ligand binding effectively through a single long α-helix (such as in dimeric Mb) compared to through the subunit surfaces (such as in Hb) [65], since the propagation of structural change starting at each heme site upon binding of a ligand

may be damped at the long α-helix due to its flexibility, making the other heme site maintain its structure.

In summary, the ν_{CO}, ν_{Fe-His}, and ν_{Fe-C} frequencies were similar between monomeric and dimeric MbCO. The relaxation rate constant of the γ_7 band of Mb after CO photo-dissociation was also similar between the monomer and dimer. These results show that the active site structure of monomeric and dimeric MbCO was very similar. However, the CO rebinding rate constant of the dimer was twice larger than that of the monomer. The increase in the size of the channel between the Xe3 cavity and the solvent by the dimerization may allow CO to migrate faster from the solvent, and thus increase the k_{on} value. The present results show that a spectroscopic investigation of dimeric Mb may provide new insights into the dynamics of Mb, owing to the similarity in the active site structure with that of the monomer with slight differences at the Xe3 cavity.

Acknowledgements

We give thanks to Mr. Leigh McDowell for his advice during manuscript preparation. This work was partially supported by Grants-in-Aid for Scientific Research from JSPS (Young Scientists B, No. 24750163 (S.N.) and Category B, No. 26288080 (S.H.)). This

study was also supported by the Green Photonics Project at NAIST sponsored by MEXT.

REFERENCES

1. Antonini E, Brunori M (1971) Hemoglobin and myoglobin in their reactions with ligands. North-Holland Publishing, Amsterdam
2. Kitagawa T, Ozaki Y (1987) Struct Bonding 64:71-114
3. Springer BA, Sligar SG, Olson JS, Phillips GN (1994) Chem Rev 94:699-714
4. Brunori M, Gibson QH (2001) EMBO Rep 2:674-679
5. Sono M, Andersson LA, Dawson JH (1982) J Biol Chem 257:8308-8320
6. Kendrew JC, Dickerson RE, Strandberg BE, Hart RG, Davies DR, Phillips DC, Shore VC (1960) Nature 185:422-427
7. Phillips SE (1978) Nature 273:247-248
8. Nagao S, Osuka H, Yamada T, Uni T, Shomura Y, Imai K, Higuchi Y, Hirota S (2012) Dalton Trans 41:11378-11385
9. Nurizzo D, Silvestrini MC, Mathieu M, Cutruzzola F, Bourgeois D, Fulop V, Hajdu J, Brunori M, Tegoni M, Cambillau C (1997) Structure 5:1157-1171
10. Crane BR, Rosenfeld RJ, Arvai AS, Ghosh DK, Ghosh S, Tainer JA, Stuehr DJ,

Getzoff ED (1999) EMBO J 18:6271-6281

11. Czjzek M, Letoffe S, Wandersman C, Delepierre M, Lecroisey A, Izadi-Pruneyre N (2007) J Mol Biol 365:1176-1186

12. Hirota S, Hattori Y, Nagao S, Taketa M, Komori H, Kamikubo H, Wang Z, Takahashi I, Negi S, Sugiura Y, Kataoka M, Higuchi Y (2010) Proc Natl Acad Sci USA 107:12854-12859

13. Hayashi Y, Nagao S, Osuka H, Komori H, Higuchi Y, Hirota S (2012) Biochemistry 51:8608-8616

14. Parui PP, Deshpande MS, Nagao S, Kamikubo H, Komori H, Higuchi Y, Kataoka M, Hirota S (2013) Biochemistry 52:8732-8744

15. Bennett MJ, Choe S, Eisenberg D (1994) Proc Natl Acad Sci USA 91:3127-3131

16. Liu Y, Hart PJ, Schlunegger MP, Eisenberg D (1998) Proc Natl Acad Sci USA 95:3437-3442

17. Liu Y, Eisenberg D (2002) Protein Sci 11:1285-1299

18. Olson JS (1981) Methods Enzymol 76:631-651

19. Rohlfs RJ, Mathews AJ, Carver TE, Olson JS, Springer BA, Egeberg KD, Sligar SG (1990) J Biol Chem 265:3168-3176

20. Li T, Quillin ML, Phillips GN, Jr., Olson JS (1994) Biochemistry 33:1433-1446

21. Huang X, Boxer SG (1994) Nat Struct Biol 1:226-229

22. Olson JS, Phillips GN (1996) J Biol Chem 271:17593-17596

23. Schlichting I, Berendzen J, Phillips GN, Jr., Sweet RM (1994) Nature 371:808-812

24. Teng TY, Srajer V, Moffat K (1994) Nat Struct Biol 1:701-705

25. Hartmann H, Zinser S, Komninos P, Schneider RT, Nienhaus GU, Parak F (1996) Proc Natl Acad Sci USA 93:7013-7016

26. Srajer V, Teng T, Ursby T, Pradervand C, Ren Z, Adachi S, Schildkamp W, Bourgeois D, Wulff M, Moffat K (1996) Science 274:1726-1729

27. Chu K, Vojtchovsky J, McMahon BH, Sweet RM, Berendzen J, Schlichting I (2000) Nature 403:921-923

28. Srajer V, Ren Z, Teng TY, Schmidt M, Ursby T, Bourgeois D, Pradervand C, Schildkamp W, Wulff M, Moffat K (2001) Biochemistry 40:13802-13815

29. Schmidt M, Nienhaus K, Pahl R, Krasselt A, Anderson S, Parak F, Nienhaus GU, Srajer V (2005) Proc Natl Acad Sci USA 102:11704-11709

30. Tomita A, Sato T, Ichiyanagi K, Nozawa S, Ichikawa H, Chollet M, Kawai F, Park SY, Tsuduki T, Yamato T, Koshihara SY, Adachi S (2009) Proc Natl Acad Sci USA 106:2612-2616

31. Tomita A, Kreutzer U, Adachi S, Koshihara SY, Jue T (2010) J Exp Biol 213:2748-2754

32. Dadusc G, Ogilvie JP, Schulenberg P, Marvet U, Miller RJ (2001) Proc Natl Acad Sci USA 98:6110-6115

33. Ishikawa H, Uchida T, Takahashi S, Ishimori K, Morishima I (2001) Biophys J 80:1507-1517

34. Sakakura M, Yamaguchi S, Hirota N, Terazima M (2001) J Am Chem Soc 123:4286-4294

35. Nishihara Y, Sakakura M, Kimura Y, Terazima M (2004) J Am Chem Soc 126:11877-11888

36. Alben JO, Caughey WS (1968) Biochemistry 7:175-183

37. Coughey WS, Alben JO, McCoy S, Boyer SH, Charache S, Hathaway P (1969) Biochemistry 8:59-62

38. Bangcharoenpaurpong O, Schomacker KT, Champion PM (1984) J Am Chem Soc 106:5688-5698

39. Spiro TG, Czernuszewicz RS, Li XY (1990) Coordin Chem Rev 100:541-571

40. Hu SZ, Smith KM, Spiro TG (1996) J Am Chem Soc 118:12638-12646

41. Unno M, Christian JF, Olson JS, Sage JT, Champion PM (1998) J Am Chem Soc

120:2670-2671

42. Yeh SR, Han SW, Rousseau DL (1998) Acc Chem Res 31:727-736

43. Mizutani Y, Kitagawa T (2001) J Phys Chem B 105:10992-10999

44. Couture M, Burmester T, Hankeln T, Rousseau DL (2001) J Biol Chem 276:36377-36382

45. Yamada K, Ishikawa H, Mizutani Y (2012) J Phys Chem B 116:1992-1998

46. Murakawa Y, Nagai M, Mizutani Y (2012) J Am Chem Soc 134:1434-1437

47. Henry ER, Sommer JH, Hofrichter J, Eaton WA (1983) J Mol Biol 166:443-451

48. Carver TE, Rohlfs RJ, Olson JS, Gibson QH, Blackmore RS, Springer BA, Sligar SG (1990) J Biol Chem 265:20007-20020

49. Gibson QH (1956) J Physiol 134:112-122

50. Findsen EW, Scott TW, Chance MR, Friedman JM, Ondrias MR (1985) J Am Chem Soc 107:3355-3357

51. Franzen S, Bohn B, Poyart C, Martin JL (1995) Biochemistry 34:1224-1237

52. Mizutani Y, Kitagawa T (1997) Science 278:443-446

53. Peterson ES, Friedman JM, Chien EY, Sligar SG (1998) Biochemistry 37:12301-12319

54. Bolognesi M, Cannillo E, Ascenzi P, Giacometti GM, Merli A, Brunori M (1982)

J Mol Biol 158:305-315

55. Ringe D, Petsko GA, Kerr DE, Ortiz de Montellano PR (1984) Biochemistry 23:2-4

56. Blouin GC, Olson JS (2010) Biochemistry 49:4968-4976

57. Smith RD, Blouin GC, Johnson KA, Phillips GN, Jr., Olson JS (2010) Biochemistry 49:4977-4986

58. Scott EE, Gibson QH, Olson JS (2001) J Biol Chem 276:5177-5188

59. Olson JS, Soman J, Phillips GN (2007) IUBMB Life 59:552-562

60. Salter MD, Blouin GC, Soman J, Singleton EW, Dewilde S, Moens L, Pesce A, Nardini M, Bolognesi M, Olson JS (2012) J Biol Chem 287:33163-33178

61. Elber R, Karplus M (1990) J Am Chem Soc 112:9161-9175

62. Mizutani Y, Kitagawa T (2001) Chem Rec 1:258-275

63. Kitagawa T, Nagai K, Tsubaki M (1979) FEBS Lett 104:376-378

64. Stein P, Mitchell M, Spiro TG (1980) J Am Chem Soc 102:7795-7797

65. Perutz MF, Wilkinson AJ, Paoli M, Dodson GG (1998) Annu Rev Biophys Biomol Struct 27:1-34

Figure Legends

Fig. 1. Crystal structures of monomeric (**a** and **b**; gray) (PDB: 1WLA) and dimeric (**c** and **d**; pink and cyan) (PDB: 3VM9) horse metMb. Whole structures of monomeric **(a)** and dimeric **(c)** metMb are shown with the active site structures of monomeric (**b**) and dimeric **(d)** metMb. Side-chain atoms of His93 and His64, and the heme are shown as stick models.

Fig. 2. Optical absorption (**a**) and CD **(b)** spectra of monomeric (blue) and dimeric (red) horse MbCO. Measurement conditions: sample concentration (heme unit), 5 μM; buffer, 50 mM potassium phosphate buffer; pH, 7.0; temperature, 20°C.

Fig. 3. FT-IR spectra of monomeric (**a**) and dimeric **(b)** horse MbCO. Measurement conditions: frequency range, 1900 to 2000 cm^{-1}; resolution, 2 cm^{-1}; cell pathlength, 20 μm; integration, 512 scans; temperature, room temperature.

Fig. 4. RR spectra of the monomer (blue) and dimer (red) of horse deoxyMb **(a)** and MbCO **(b)**. Measurement conditions: Mb concentration (heme unit), 75 μM (monomeric deoxyMb, monomeric MbCO, and dimeric MbCO), and 100 μM (dimeric

deoxyMb); buffer, 50 mM potassium phosphate buffer; pH, 7.0; temperature, room temperature.

Fig. 5. Time-resolved RR spectra of CO photo-dissociated monomeric (**a** and **c**) and dimeric horse Mb (**b** and **d**). The γ_7 band in the RR spectra of monomeric (**c**) and dimeric (**d**) CO photo-dissociated Mb is shown. Each spectrum of the γ_7 band was measured at 50 (purple), 100 (blue), 150 (light blue), 200 (green), 300 (light green), 400 (orange), and 500 (red) ns after CO dissociation. (Inset) Plots of the peak area of the γ_7 band after CO photo-dissociation, together with the single exponential best-fitted curve. The peak areas are normalized by fixing the peak area at 50 ns to 1. Measurement conditions: Mb concentration (heme unit), 75 μM; buffer, 50 mM potassium phosphate buffer; pH, 7.0; temperature, room temperature.

Fig. 6. Flash-photolysis measurements of monomeric (blue) and dimeric (red) horse MbCO. Absorbance changes at 435 nm by 532-nm pulse irradiation under various CO concentrations are shown. Single exponential best-fitted curves are indicated by red broken lines. (Inset) Plots of k_{obs} vs. [CO] for the reaction of Mb with CO, together with the least-squares-fitted line according to eq. 1. Measurement conditions: sample

concentration, 8 μM (heme unit); buffer, 50 mM potassium phosphate buffer; pH, 7.0; temperature, 20°C; laser pulse power, 5 mJ; laser pulse frequency, 10 Hz; [CO]: 0.21, 0.41, 0.62, 0.82, and 1.03 mM (remaining gas is N_2).

Fig. 7. Superimposed structures of monomeric (PDB: 1WLA) and dimeric (PDB: 3VM9) horse metMb. Protein structures of monomeric (gray) and dimeric (pink and cyan) Mb are shown. Xe atoms (Xe1-Xe4; orange sphere) are inserted into the positions obtained from the metMb structure determined at high Xe pressures (PDB: 2W6W). The key amino acid residues and heme are shown as stick model. The changes in the positions of the side chains of Trp7, His82, and Leu137 of Mb by the dimerization are indicated with blue arrows.

Figure 1

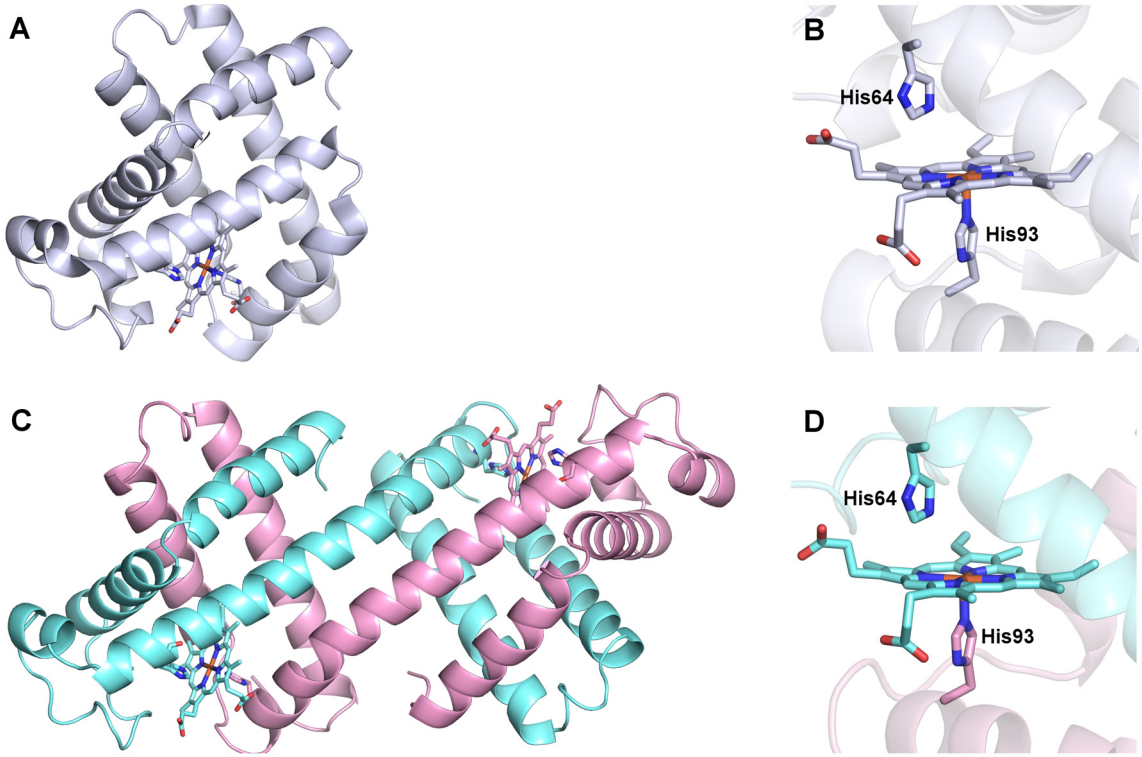

Figure 2

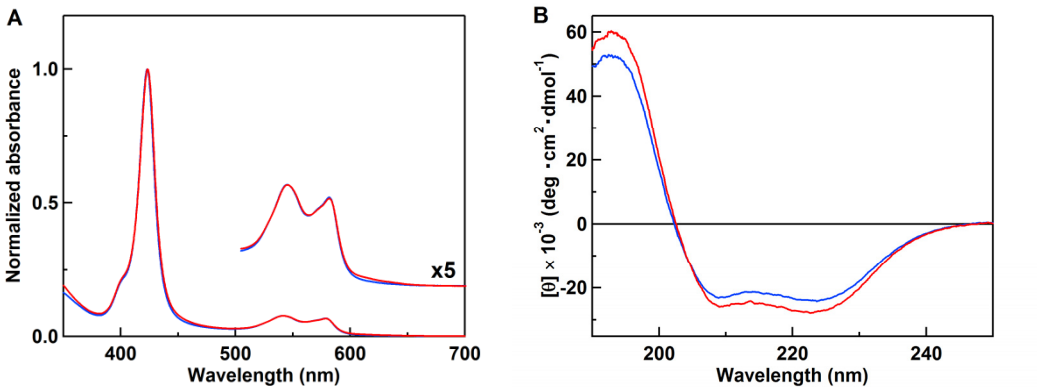
A
Normalized absorbance
1.0
0.5
0.0
400
500
600
700
Wavelength (nm)
x5
B
60
40
20
0
-20
[θ] × 10^-3 (deg ·cm^2 ·dmol^-1)
200
220
240
Wavelength (nm)

1 Figure 3

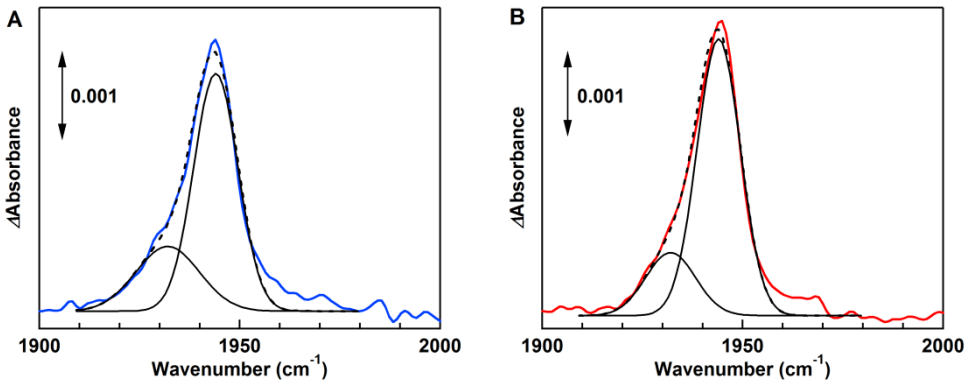
A
0.001
ΔAbsorbance
1900
1950
2000
Wavenumber (cm-1)
B
0.001
ΔAbsorbance
1900
1950
2000
Wavenumber (cm-1)

2

3

Figure 4

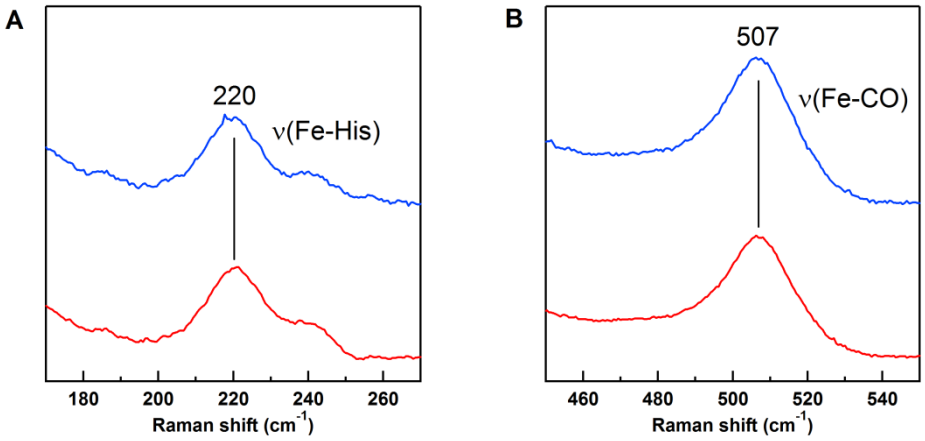
A
220
ν(Fe-His)
180
200
220
240
260
Raman shift (cm-1)
B
507
ν(Fe-CO)
460
480
500
520
540
Raman shift (cm-1)

Figure 5

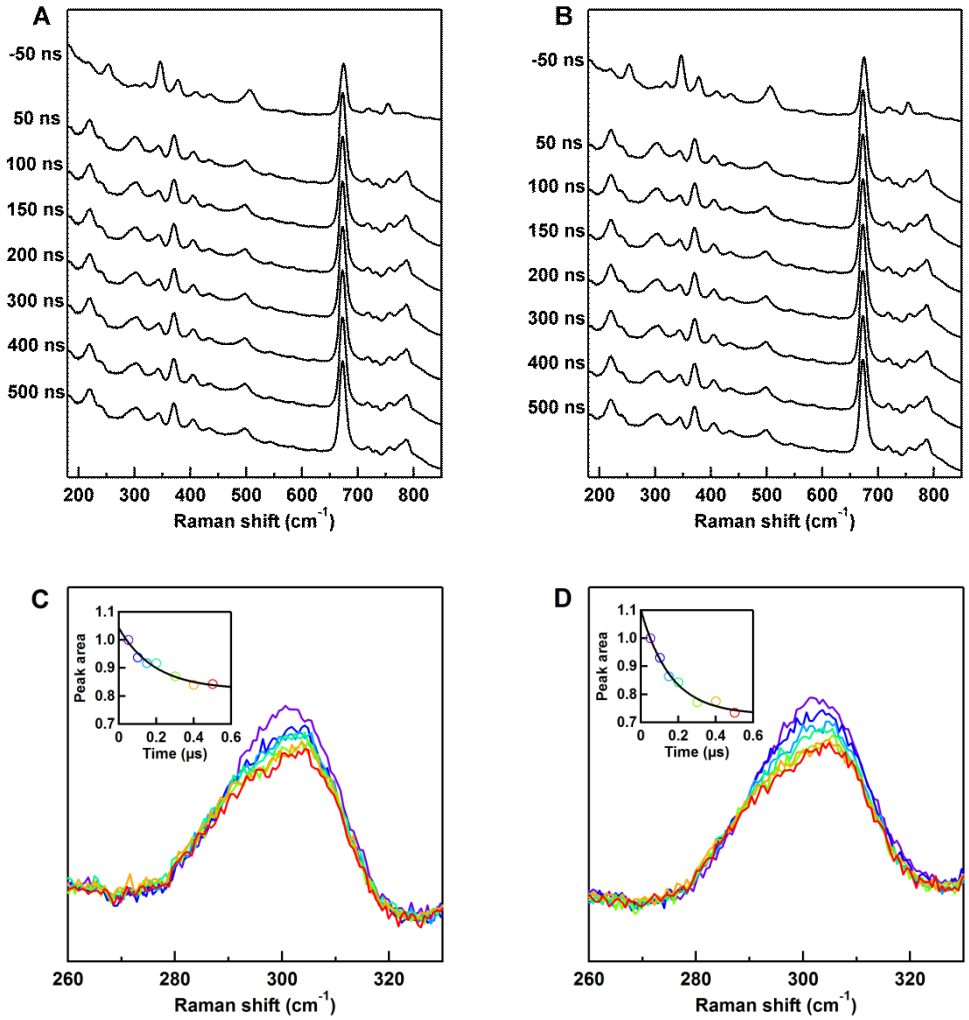
A
-50 ns
50 ns
100 ns
150 ns
200 ns
300 ns
400 ns
500 ns
200 300 400 500 600 700 800
Raman shift (cm-1)
B
-50 ns
50 ns
100 ns
150 ns
200 ns
300 ns
400 ns
500 ns
200 300 400 500 600 700 800
Raman shift (cm-1)
C
Peak area
1.1 1.0 0.9 0.8 0.7
0 0.2 0.4 0.6
Time (μs)
260 280 300 320
Raman shift (cm-1)
D
Peak area
1.1 1.0 0.9 0.8 0.7
0 0.2 0.4 0.6
Time (μs)
260 280 300 320
Raman shift (cm-1)

1 Figure 6

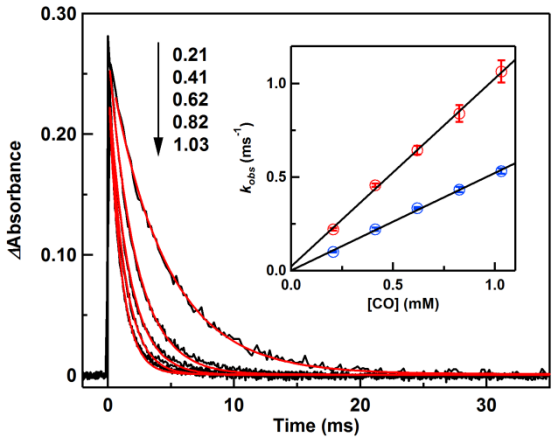

2

3

4

Figure 7

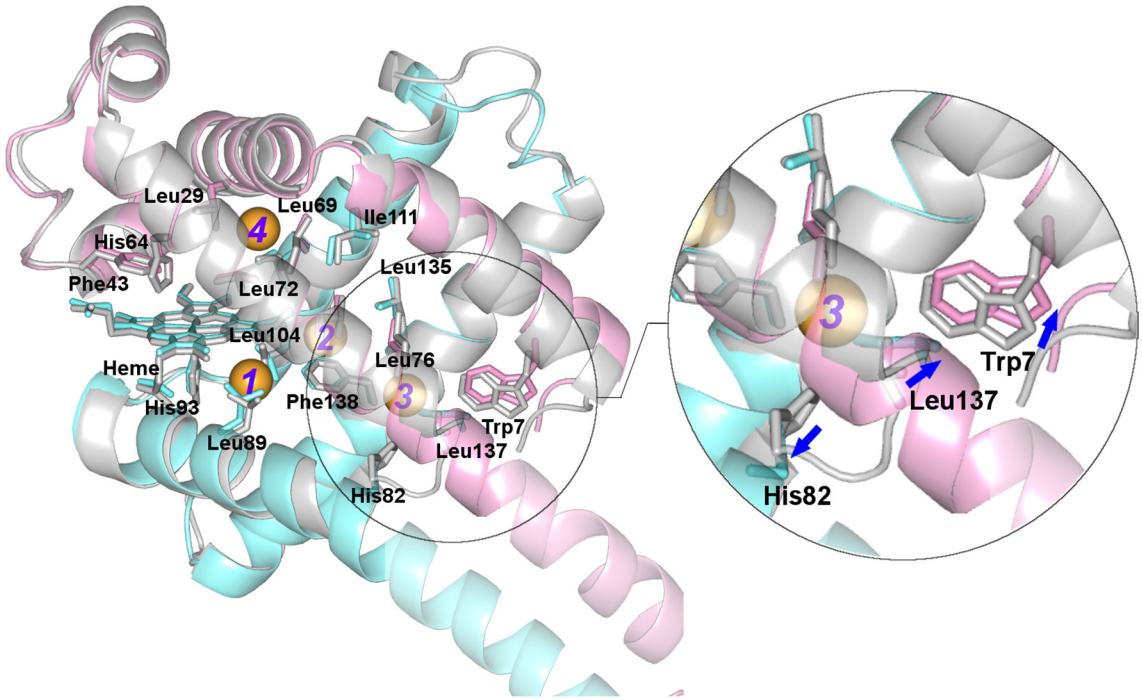
Leu29
Leu69
Ile111
His64
Leu135
Phe43
Leu72
Leu104
Heme
Leu76
His93
Phe138
Trp7
Leu89
Leu137
His82
Trp7
Leu137
His82

Supplementary Material

Carbon monoxide binding properties of domain-swapped dimeric myoglobin

Satoshi Nagao • Haruto Ishikawa • Takuya Yamada • Yasuhisa Mizutani • Shun Hirota

S. Nagao • T. Yamada • S. Hirota (✉)
Graduate School of Materials Science, Nara Institute of Science and Technology, 8916-5, Takayama, Ikoma, Nara 630-0192, Japan
E-mail: hirota@ms.naist.jp; Fax: +81-743-72-6119, Tel: +81-743-72-6110

H. Ishikawa · Y. Mizutani
Department of Chemistry, Graduate School of Science, Osaka University, 1-1 Machikaneyama, Toyonaka 560-0043, Japan

Contents

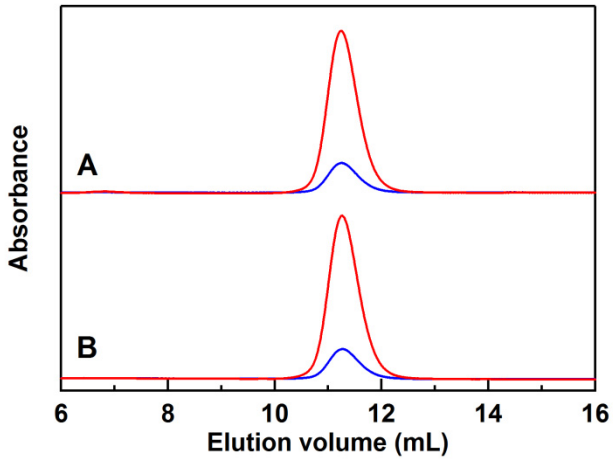

Figure S1. Size exclusion chromatographs of dimeric Mb. **a** Dimeric horse metMb after reduction with dithionite under CO atmosphere. **b** Dimeric metMb before treatment. Gel chromatographic conditions: Column, Superdex 75 10/300 GL; flow rate, 0.5 mL/min; monitoring wavelength, 280 (blue) and 423 (red) nm; solvent, 50 mM potassium phosphate buffer, pH 7.0; temperature, 4°C.

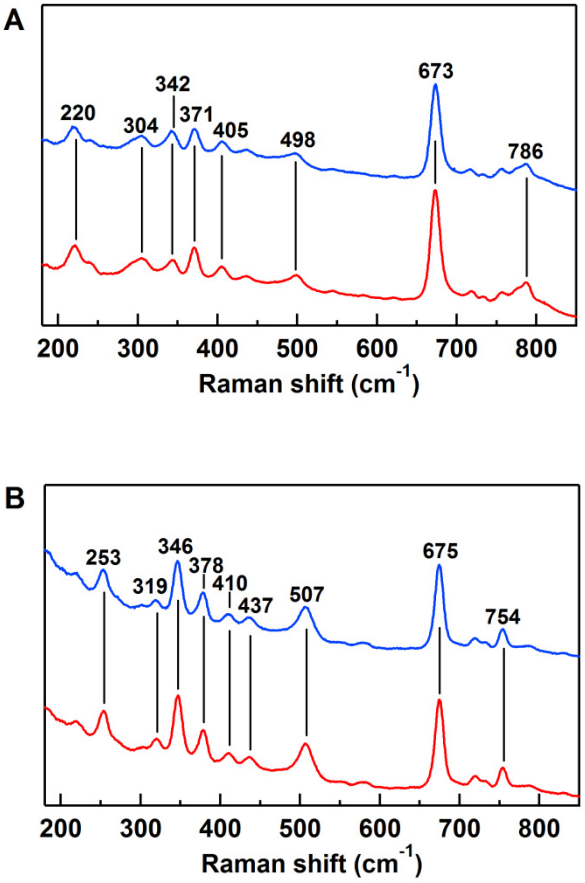

Figure S2. RR spectra of the monomer (blue) and dimer (red) of deoxyMb (**a**) and MbCO (**b**). Measurement conditions: Mb concentration (heme unit), 75 μM (monomeric deoxyMb, dimeric deoxyMb, and dimeric MbCO) and 100 μM (dimeric deoxyMb); buffer, 50 mM potassium phosphate buffer; pH, 7.0; temperature, room temperature.